Continuum Mech. Thermodyn.
DOI 10.1007/s00161-011-0202-0

ORIGINAL ARTICLE

Henning Struchtrup

Resonance in rarefied gases

Received: 2 September 2011 / Accepted: 13 September 2011

Abstract Dispersion and damping of ultrasound waves are a standard test for mathematical models of rarefied gas flows. Normally, one considers waves in semi-infinite systems in relatively large distance of the source. For a more complete picture, ultrasound propagation in finite closed systems of length L is studied by means of several models for rarefied gas flows: the Navier-Stokes-Fourier equations, Grad's 13 moment equations, the regularized 13 moment equations, and the Burnett equations. All systems of equations are considered in simple 1-D geometry with their appropriate jump and slip boundary conditions. Damping and resonance are studied in dependence of frequency and length. For small L, all wave modes contribute to the solution.

Keywords Rarefied gases · Dispersion relation · Non-equilibrium thermodynamics · Extended thermodynamics

1 Introduction

The Navier-Stokes and Fourier equations of classical hydrodynamics describe gas flows only accurately when the Knudsen number Kn is sufficiently small. Usually the Knudsen number is defined as the ratio between particle mean free path and a relevant process length, but for time-dependent problems it can be equivalently defined as the ratio between the particle mean free time and a relevant process time scale, e.g. the duration of an oscillation. In the following we shall consider rarefied gases in short ultrasound resonators which have two relevant Knudsen numbers, one based on the resonator length, and the other on the oscillator frequency.

When the process Knudsen number exceeds a value of about 0.1, the equations of classical hydrodynamics cannot predict speed of sound and damping of ultrasound waves accurately and thus they fail in the description of ultrasound resonators. Therefore, the description of ultrasound resonators must be based on more refined theories, which can be derived from kinetic theory of gases [1–4]. The most accurate description comes from the Boltzmann equation itself, which describes the gas on the microscopic level, and is valid for all Knudsen numbers. However, its mathematical complexity makes the description cumbersome, and numerical simulations costly.

As long as the Knudsen number is not too large, refined macroscopic transport equations can be derived from the Boltzmann equation which allow the accurate description of processes at much lower mathematical or numerical cost than the Boltzmann equation [4,5]. There are two main approaches to macroscopic transport equations for rarefied gases, the Chapman–Enskog expansion and moment methods.

Dedicated to Prof. Ingo Müller on the occasion of his 75th birthday.

Communicated by Manuel Torrilhon.

H. Struchtrup (✉)
University of Victoria, Victoria, BC, Canada
E-mail: struchtr@uvic.ca

Published online: 11 October 2011

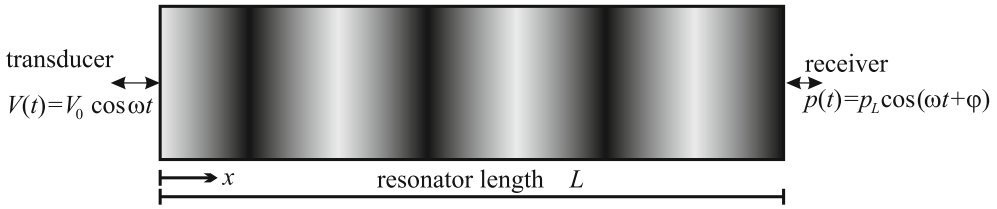

Fig. 1 The resonator of length L is driven periodically with frequency ω by the transducer on the *left*. The receiver on the *right* measures the pressure amplitude p_L and the phase shift φ

In the Chapman–Enskog method, one expands the Boltzmann equation to derive refined constitutive laws for stress and heat flux which add higher gradient terms to the Navier-Stokes and Fourier laws. The resulting Burnett and super-Burnett equations [6,7] are not usable as simulation tool since they suffer from instabilities in initial value problems [8], and there is no complete theory for their boundary conditions. In the following, we shall consider the Burnett equations, with new boundary conditions based on those for the R13 equations (see below). In the periodic resonator, initial values are not relevant, and thus instabilities are not observed. However, also for pure boundary value problems the Burnett equations yield modes which are unphysical—these will be discussed briefly.

In moment methods one extends the space of hydrodynamic variables by adding full balance equations for stress, heat flux and other quantities. Some theories of this type are also known as "Extended Thermodynamics" [9] or "Generalized Hydrodynamics" [10], where different schools propose different constitutive equations for the closure of the additional balance laws. The best-known example of moment equations is Grad's 13 moment (G13) equations [11,12]. A more recent development is the regularized 13 moment (R13) equations, which add higher-order terms to the G13 equations and thus extend their validity towards higher Knudsen numbers [4,13,14]. The R13 equations are accompanied by a full theory of boundary conditions [15]. In a number of recent publications it was shown that the R13 equations deliver fairly accurate descriptions of rarefied flows for Knudsen numbers below 0.5 including Knudsen boundary layers, non-Fourier heat flux, etc; due to space limitations, the reader is referred to the pertinent literature for details [13–21].

In the following we shall consider the Navier-Stokes-Fourier (NSF) equations, the Burnett equations, G13 equations and the R13 equations for short ultrasound resonators. All sets of equations yield several wave modes, and the full solution for the resonator is a superposition of all modes, where the amplitudes of the modes are due to the boundary conditions. When discussing damping and phase speed of ultrasound waves, it is common to consider only the so-called acoustic mode [4,9,22], while all other modes are ignored. Our calculations allow to understand the importance—or, indeed, unimportance—of the additional modes. It will be seen that the R13 equations agree best with resonator measurements by Schotter [23].

2 The resonator

2.1 Set-up and notation

Figure 1 shows a sketch of the resonator geometry. A rarefied gas is enclosed between two walls at distance L, measured along the x -coordinate. One wall is the transducer which imposes the periodic velocity $V(t) = V_0 \cos \omega t$. The other wall is the resting receiver where the gas pressure is measured. Pressure must show the same periodicity as velocity, but one will expect a phase shift φ, so that the measured signal is $p(t) = p_L \cos(\omega t + \varphi_L)$.

The gas rest state is given by density ρ_0 and temperature in energy units $\theta_0 = \mathcal{R}T_0$ ($\mathcal{R}$ is the gas constant and T denotes thermodynamic temperature). The velocity amplitude V_0 is so small that the gas is only slightly disturbed, therefore it is sufficient to consider all transport equations in linearized form. The dimensions perpendicular to the $x-$direction are much bigger than L, so that the processes in the resonator can be described as one-dimensional: all fields depend only on time t and location x.

In the experiment, one controls velocities and temperatures at the transducer ($x = 0$) and at the receiver ($x = L$), the corresponding wall velocities, temperatures and wall normals n (points into the gas) are

$$\begin{array}{lll} \text{at } x = 0 \ : \ v_W(t) = V_0 \cos \omega t, & \theta_W(t) = \theta_0, & n = 1 \\ \text{at } x = L \ : \ v_W(t) = 0, & \theta_W(t) = \theta_0 & n = -1 \end{array} \tag{1}$$

2.2 Dimensionless quantities

In the following, dimensionless quantities will be used exclusively, which are defined through the rest state ρ_0, θ_0 as

$$\tilde{x} = \frac{x}{L_0}, \quad \tilde{t} = \sqrt{\theta_0}\frac{t}{L_0}, \quad \mathrm{Kn} = \frac{\mu_0\sqrt{\theta_0}}{p_0 L_0},$$
$$\tilde{\rho} = \frac{\rho}{\rho_0} - 1, \quad \tilde{v} \to \frac{v}{\sqrt{\theta_0}}, \quad \tilde{\theta} = \frac{\theta}{\theta_0} - 1, \quad \tilde{\sigma} = \frac{\sigma}{p_0}, \quad \tilde{q} = \frac{q}{p_0\sqrt{\theta_0}}$$

Here, x and t denote space and time, and the thermodynamic quantities are: density ρ, velocity v, temperature θ, stress σ, heat flux q. All quantities with tilde are defined as dimensionless deviations from the ground state; the tildes will be omitted in the subsequent equations for better readability.

The viscosity at reference temperature is μ_0 and the Knudsen number Kn is a measure for the ratio between the mean free path $\lambda_0 = \frac{\mu_0\sqrt{\theta_0}}{p_0}$ of the gas, and a characteristic length L_0 of the problem. Note that these definitions of mean free path and Knudsen number differ by a factor $\sqrt{\frac{\pi}{2}}$ from that commonly used [2]; for the macroscopic equations in kinetic theory the above definition is most convenient, and this is why we use it.

To avoid confusion, we rewrite the boundary conditions (1) in the dimensionless variables, where they read

$$\begin{aligned} &\text{at } x = 0 \ : \ \tilde{v}_W(t) = V_0 \cos\omega t, \quad \tilde{\theta}_W(t) = 0, \quad n = 1 \\ &\text{at } x = L \ : \ \tilde{v}_W(t) = 0, \qquad\qquad \tilde{\theta}_W(t) = 0 \quad n = -1 \end{aligned} \tag{2}$$

2.3 Frequency, length and Knudsen number

The resonator is characterized by two relevant measures, the resonator length L, and the frequency ω, which both can be used to define a Knudsen number. However, it is most convenient for the calculations to set $\mathrm{Kn} = 1$, so that the characteristic length L_0 is the mean free path,

$$L_0 = \frac{\mu_0\sqrt{\theta_0}}{p_0} = \lambda_0.$$

Then, the characteristic time becomes

$$t_0 = \frac{L_0}{\sqrt{\theta_0}} = \frac{\mu_0}{p_0} = \tau_0,$$

that is, time is measured in units of the mean free time τ_0 [4]. Accordingly, resonator length L and frequency ω are made dimensionless as

$$\tilde{L} = \frac{L}{\lambda_0}, \quad \tilde{\omega} = \omega\tau_0 = \frac{\tau_0}{\frac{1}{\omega}}.$$

Thus, the dimensionless resonator length is an inverse Knudsen number, and the dimensionless frequency can be considered as a Knudsen number itself, e.g. by writing

$$\tilde{L} = \frac{L}{\lambda_0} = \frac{1}{\mathrm{Kn}_L}, \quad \tilde{\omega} = \frac{\tau_0}{\frac{1}{\omega}} = \mathrm{Kn}_\omega.$$

All macroscopic equations discussed below are valid only for sufficiently low Knudsen numbers. From the above discussion follows that resonator length must be sufficiently large and frequency must be sufficiently low for this condition to hold. What values are sufficient will become clear from the discussion.

3 Moment equations and boundary conditions

3.1 Conservation laws in 1-D

All sets of macroscopic transport equations considered include the conservation laws for mass, momentum and energy, which read in dimensionless, linearized form and 1-D geometry [4]

$$\begin{aligned} \frac{\partial \rho}{\partial t} + \frac{\partial v}{\partial x} &= 0, \\ \frac{\partial v}{\partial t} + \frac{\partial \rho}{\partial x} + \frac{\partial \theta}{\partial x} + \frac{\partial \sigma}{\partial x} &= 0, \\ \frac{3}{2}\frac{\partial \theta}{\partial t} + \frac{\partial q}{\partial x} + \frac{\partial v}{\partial x} &= 0. \end{aligned} \tag{3}$$

The factor $\frac{3}{2}$ in the energy balance is the dimensionless specific heat, the value is that for monatomic gases, which are considered exclusively.

The variables in the conservation laws are mass density ρ, velocity in x-direction v and temperature θ. In addition, the equations contain the xx-component of the viscous stress, σ and the x-component of the heat flux, q. The various theories for transport provide equations for stress and heat flux which are presented in the following sections, together with their appropriate boundary conditions.

3.2 NSF equations

The Navier-Stokes and Fourier equations can be derived from the Boltzmann equation by Chapman–Enskog expansion to first order in the Knudsen number. In dimensionless form and 1-D geometry, stress and heat flux are given by

$$\frac{4}{3}\frac{\partial v}{\partial x} = -\frac{\sigma}{\mathrm{Kn}}, \quad \frac{5}{2}\frac{\partial \theta}{\partial x} = -\frac{2}{3}\frac{q}{\mathrm{Kn}}. \tag{4}$$

The appropriate boundary conditions are derived from the boundary conditions for the Boltzmann equation and the distribution function found in the Chapman–Enkog expansion as [4,16]

$$\begin{aligned} v &= v_W\,(t), \\ \theta - \mathrm{Kn}\frac{1}{3}\frac{\partial v}{\partial x} - \mathrm{Kn}\frac{2-\chi}{2\chi}\sqrt{\frac{\pi}{2}}\frac{15}{4}\frac{\partial \theta}{\partial x}n &= \theta_W\,(t). \end{aligned} \tag{5}$$

Here, χ is the accommodation coefficient which describes the interaction between gas particles and wall. The boundary conditions are based on Maxwell's accommodation model, where it is assumed that particles are either fully thermalized at the wall, or specularly reflected [2,24]; χ is the percentage of particles that thermalize.

The first condition is just the statement that the normal velocity of the gas is equal to the normal velocity at the wall, so that there is no mass flux into the wall, the second is the jump condition for temperature. Due to the simple one-dimensionality of the process, a slip condition for velocity as it is needed for shear flows is not required. The boundary conditions must be evaluated at transducer and receiver with the values for v_W, θ_W and n given in (2).

We left the Knudsen number in the above equations since it shows the scaling of the various terms at a glance: stress, heat flux and temperature jump are all of first order in the Knudsen number. For the same reason we shall keep the Knudsen number in the other equations below; for all computations we shall rescale so that $\mathrm{Kn} = 1$.

3.3 G13 equations

Grad's 13 moment equations are valid up to second order in Kn; for details of their derivation we refer the reader to the original works of Grad [11,12]; for proof that they are indeed of second order see [4,14]. In the Grad equations, stress and heat flux are not given as constitutive laws anymore, but they are thermodynamic variables in their own right, with the balance equations

$$\frac{\partial \sigma}{\partial t} + \frac{8}{15}\frac{\partial q}{\partial x} + \frac{4}{3}\frac{\partial v}{\partial x} = -\frac{\sigma}{\mathrm{Kn}}, \quad \frac{\partial q}{\partial t} + \frac{\partial \sigma}{\partial x} + \frac{5}{2}\frac{\partial \theta}{\partial x} = -\frac{2}{3}\frac{q}{\mathrm{Kn}}. \tag{6}$$

Note that the terms adjacent to the equal signs are just the NSF constitutive laws (4). Indeed, by first-order Chapman–Enskog expansion the G13 equations reduce to NSF [4].

In the resonator geometry, the linear G13 equations require as many boundary conditions as the NSF equations. The appropriate conditions are

$$\begin{aligned} v &= v_W\,(t), \\ \theta + \frac{1}{4}\sigma + \frac{2-\chi}{2\chi}\sqrt{\frac{\pi}{2}}qn &= \theta_W\,(t); \end{aligned} \tag{7}$$

these must be evaluated at transducer and receiver with (2). Note that the boundary conditions for G13 reduce to those for NSF when one inserts the NSF constitutive relations (4).

3.4 R13 equations

The R13 equations are accurate to third order in the Knudsen number, their detailed derivation is presented in [4,13,14]. The R13 equations are an extension of the G13 equations which add higher-order terms (stemming from higher-order moment equations). The dimensionless 1-D equations required for the resonator problem read [4]

$$\begin{aligned} \frac{\partial\sigma}{\partial t} + \frac{8}{15}\frac{\partial q}{\partial x} - \frac{6}{5}\mathrm{Kn}\frac{\partial^2\sigma}{\partial x^2} + \frac{4}{3}\frac{\partial v}{\partial x} &= -\frac{\sigma}{\mathrm{Kn}}, \\ \frac{\partial q}{\partial t} + \frac{\partial\sigma}{\partial x} - \frac{18}{5}\mathrm{Kn}\frac{\partial^2 q}{\partial x^2} + \frac{5}{2}\frac{\partial\theta}{\partial x} &= -\frac{2}{3}\frac{q}{\mathrm{Kn}}. \end{aligned} \tag{8}$$

These are just the G13 equations with two additional terms with second derivatives of stress and heat flux.

The full set of boundary conditions for R13 were derived and discussed in [15]. When considered for the 1-D geometry of the resonator and linearized some of the conditions reduce to mere identities and one becomes redundant, so that the only relevant boundary conditions are

$$\begin{aligned} v &= v_W\,(t), \\ \theta + \frac{1}{4}\sigma + \frac{2-\chi}{2\chi}\sqrt{\frac{\pi}{2}}qn - \frac{24}{35}\mathrm{Kn}\frac{\partial q}{\partial x} &= \theta_W\,(t), \\ \theta - \frac{7}{2}\sigma + 6\mathrm{Kn}\frac{2-\chi}{2\chi}\sqrt{\frac{\pi}{2}}\frac{\partial\sigma}{\partial x}n + \frac{6}{35}\mathrm{Kn}\frac{\partial q}{\partial x} &= \theta_W\,(t). \end{aligned} \tag{9}$$

As before, the first and second condition are just the no-flux condition at the wall and the jump condition for temperature, which now has an additional term with the heat flux derivative. Due to the higher-order derivatives in (8), the additional boundary condition $(9)_3$ is required, which is an additional jump condition for the variables. All three conditions must be evaluated at transducer and receiver with (2).

3.5 Burnett equations

The Burnett equations are derived from the second-order Chapman–Enskog expansion of the Boltzmann equation [1,6]. They can also be obtained from the second-order Chapman–Enskog expansion of the G13 or R13 equations [4]. It is well known that the Burnett equations suffer from stability problems in initial value problems [8], and there is no complete theory for their boundary conditions. The instability is not an issue for the present boundary value problem, and we shall employ the R13 boundary conditions. Thus, we can consider the Burnett equations as well.

In the linearized 1-D Burnett equations, stress and heat flux have the NSF terms and additional second-order corrections, they can be written as [4]

$$\begin{aligned} \mathrm{Kn}\left[\frac{4}{3}\frac{\partial^2\rho}{\partial x^2} - \frac{2}{3}\frac{\partial^2\theta}{\partial x^2}\right] + \frac{4}{3}\frac{\partial v}{\partial x} &= -\frac{\sigma}{\mathrm{Kn}}, \\ \frac{7}{6}\mathrm{Kn}\frac{\partial^2 v}{\partial x^2} + \frac{5}{2}\frac{\partial\theta}{\partial x} &= -\frac{2}{3}\frac{q}{\mathrm{Kn}}. \end{aligned} \tag{10}$$

Compared to NSF, the Burnett equations contain higher derivatives, and this is the reason why more boundary conditions are required. Indeed, closer examination shows that the Burnett equation needs 6 boundary conditions (3 at each side), just as the R13 equations. Thus, it appears to be natural to consider the R13 boundary conditions (9) together with the Burnett expressions for stress and heat flux (10), which yields

$$
\begin{aligned}
&v = v_W\,(t),\\
&\theta - \frac{1}{3}\mathrm{Kn}\frac{\partial v}{\partial x} - \frac{2-\chi}{2\chi}\sqrt{\frac{\pi}{2}}\frac{15}{4}\mathrm{Kn}\frac{\partial \theta}{\partial x}n - \mathrm{Kn}^2\frac{1}{3}\frac{\partial^2 \rho}{\partial x^2}\\
&\quad +\mathrm{Kn}^2\frac{115}{42}\frac{\partial^2 \theta}{\partial x^2} - \frac{2-\chi}{2\chi}\sqrt{\frac{\pi}{2}}\frac{7}{4}\mathrm{Kn}^2\frac{\partial^2 v}{\partial x^2}n + \mathrm{Kn}^3\frac{6}{5}\frac{\partial^3 v}{\partial x^3} = \theta_W\,(t),
\end{aligned}
$$

$$
\begin{aligned}
&\theta + \frac{14}{3}\mathrm{Kn}\frac{\partial v}{\partial x} + \frac{14}{3}\mathrm{Kn}^2\frac{\partial^2 \rho}{\partial x^2} - \mathrm{Kn}^2\frac{125}{42}\frac{\partial^2 \theta}{\partial x^2} - 8\mathrm{Kn}^2\frac{2-\chi}{2\chi}\sqrt{\frac{\pi}{2}}\frac{\partial^2 v}{\partial x^2}n\\
&-\frac{3}{10}\mathrm{Kn}^3\frac{\partial^3 v}{\partial x^3} - \mathrm{Kn}^3 8\frac{2-\chi}{2\chi}\sqrt{\frac{\pi}{2}}\frac{\partial^3 \rho}{\partial x^3}n + 4\mathrm{Kn}^3\frac{2-\chi}{2\chi}\sqrt{\frac{\pi}{2}}\frac{\partial^3 \theta}{\partial x^3}n = \theta_W\,(t).
\end{aligned}
\tag{11}
$$

The three conditions must be evaluated at transducer and receiver with (2).

4 Resonator solution

4.1 Wave solutions

Due to the simple one-dimensional geometry and linearity, all sets of equations can be solved analytically. To treat all at the same time, we write all sets in the general form

$$
\frac{\partial u_A}{\partial t} + \mathcal{A}^{(1)}_{AB}\frac{\partial u_B}{\partial x} + \mathcal{A}^{(2)}_{AB}\frac{\partial^2 u_B}{\partial x^2} + \mathcal{A}^{(3)}_{AB}\frac{\partial^3 u_B}{\partial x^3} = -\mathcal{A}^{(0)}_{AB}u_B \tag{12}
$$

with the variable vector u_A and suitable matrices $\mathcal{A}^{(\alpha)}_{AB}$. For NSF we have $u_A = \{\rho, v, \theta\}$ and $\mathcal{A}^{(0)}_{AB} = \mathcal{A}^{(3)}_{AB} = 0$; for Burnett we have $u_A = \{\rho, v, \theta\}$ and $\mathcal{A}^{(0)}_{AB} = 0$; for G13 we have $u_A = \{\rho, v, \theta, \sigma, q\}$ and $\mathcal{A}^{(2)}_{AB} = \mathcal{A}^{(3)}_{AB} = 0$; for R13 we have $u_A = \{\rho, v, \theta, \sigma, q\}$ and $\mathcal{A}^{(3)}_{AB} = 0$.

For the solution of the periodically driven resonator we make the harmonic wave ansatz

$$
u_A\,(x,t) = \check{u}_A \exp\left[k_i x\right]\cos\left[\omega t - k_r x + \varphi\right]. \tag{13}
$$

Here, ω is the frequency of the wave as imposed at the transducer, $\check{u}_A$ and φ are amplitude and phase shift, respectively. The phase velocity of the wave is $v_{ph} = \frac{\omega}{k_r}$, and the damping is $(-k_i)$. Note that for a wave with positive phase velocity (i.e. $k_r > 0$), one will expect a positive damping (i.e. $k_i < 0$).

For the calculation it is convenient to consider the complex representation of the wave

$$
u_A\,(x,t) = \hat{u}_A \exp\left[i\,(\omega t - kx)\right], \tag{14}
$$

where ω is the real frequency, $k = k_r + ik_i$ is the complex wave number and $\hat{u}_A = \check{u}_A \exp\left[i\varphi\right]$ is the complex amplitude. It is understood that only the real part of (14) is relevant.

Inserting the wave ansatz (14) into the general form of the transport equations and performing all derivatives gives the algebraic equation

$$
\left(\delta_{AB} i\omega + \mathcal{A}^{(0)}_{AB} - ik\mathcal{A}^{(1)}_{AB} - k^2\mathcal{A}^{(2)}_{AB} + ik^3\mathcal{A}^{(3)}_{AB}\right)\hat{u}_B = \mathfrak{A}_{AB}\,(k)\,\hat{u}_B = 0, \tag{15}
$$

which only has non-trivial solutions $\hat{u}_B$ for the complex amplitudes if the determinant of the matrix $\mathfrak{A}_{AB}\,(k)$ vanishes,

$$
\det\left[\mathfrak{A}_{AB}\,(k)\right] \stackrel{!}{=} 0\,. \tag{16}
$$

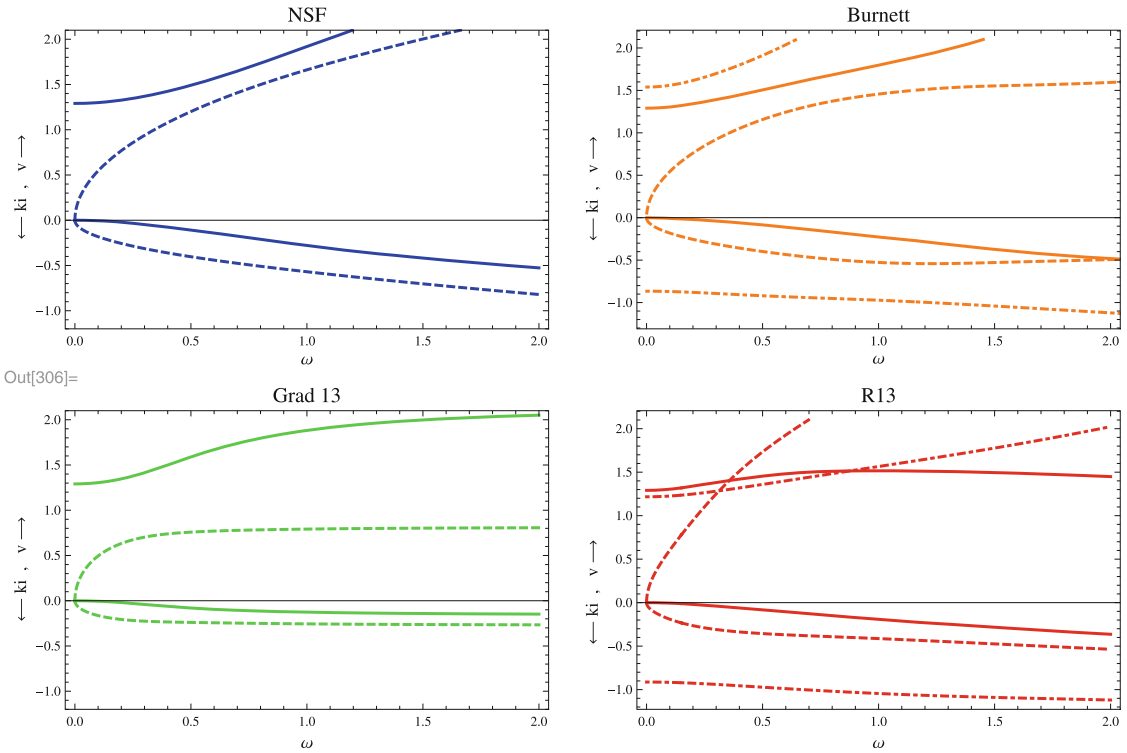

Fig. 2 The branches of the dispersion relation for NSF, Burnett, G13, R13 as function of frequency ω. Only solutions travelling into positive direction are shown. Positive values are the phase speeds $v_{ph} = \frac{\omega}{k_i}$, negative values are the corresponding damping coefficients k_i. We distinguish acoustic mode (*continuous lines*), heat transfer mode (*dashed lines*) and rarefaction mode (*dotted lines*, Burnett and R13 only)

Due to the polynomial structure of the complex matrix $\mathfrak{A}_{AB}(k)$, its determinant is a polynomial of degree ν in k, with $\nu = 4$ for NSF and G13, and $\nu = 6$ for R13 and Burnett. Solution of the solvability condition (16) gives the ν branches of the dispersion relation

$$k_a(\omega), \quad a = 1, \ldots, \nu. \tag{17}$$

Only for these values of k is the solution non-trivial. The complex amplitude vector $\hat{u}_B$ must be a corresponding null-vector R_B; we write

$$\hat{u}_B(k_a(\omega)) = R_B^a(\omega) \quad \text{with} \quad \mathfrak{A}_{AB}(k_a(\omega)) R_B^a(\omega) = 0. \tag{18}$$

The general solution for the fields u_A is the superposition of the solutions for all branches of the dispersion relation,

$$u_A = \sum_{a=1}^{\nu} \alpha_a R_A^a(\omega) \exp[i(\omega t - k_a(\omega) x)]. \tag{19}$$

The ν weight factors α_a, $a = 1, \ldots, \nu$, must be determined from the boundary conditions. The computation of the dispersion relation k_a and of the null-vectors R_B^a can be done easily with commercial computer algebra systems; we used Mathematica.

4.2 Dispersion relation

Before we proceed with the solution for the resonator problem by adapting the amplitudes to the boundary conditions, we have a short glance at the dispersion relations for our four sets of equations.

For all sets, we find an even number of branches, which occur pairwise, each pair describing one wave travelling to the right and one travelling to the left with identical speed and damping. Figure 2 shows the

branches with positive phase velocity plotted over the dimensionless frequency ω. In the plots, curves with positive values are the phase velocity $v_{ph} = \frac{\omega}{k_r}$ and curves with negative values show the corresponding damping factor k_i.

For $\omega \to 0$, we find one mode with the (dimensionless) phase velocity $\sqrt{\frac{5}{3}} = 1.29$ and vanishing damping for all sets of equations (continuous lines in all figures). This is the acoustic mode which describes the propagation of weakly damped waves with the speed of sound $\sqrt{\frac{5}{3}\mathcal{R}T}$. The various sets of equations predict growing sound velocity and damping; however, the predictions differ greatly in detail, with NSF predicting the fastest increase of sound speed and damping, and R13 predicting the smallest increase of speed and even a slight decrease for $\omega > 1$. As will be seen in the proceedings, the acoustic mode is the main mode for the description of the resonator, the different predictions of the four models are mainly due to the differences in phase speed and damping of the acoustic mode.

Another mode common to all sets for small ω is a diffusive mode with, in the limit $\omega \to 0$, $k = \pm\sqrt{\frac{\omega}{3}}(1-i)$, shown in the dashed curves in the figures. This mode is more strongly damped than the acoustic mode, which is a main reason that it plays only a minor role in the resonator. Again, the four models differ widely in the details for phase speed and damping of this mode as frequency grows. In particular, all models but G13 predict growing phase speed and damping, that is the mode remains of diffusive character as frequency grows. For G13, however, due to the hyperbolic character of the equations [9] , this mode changes is character: phase speed and damping approach constant values, much like in the acoustic mode.

Only Burnett and R13 equations exhibit another mode, which has finite wavespeed for $\omega \to 0$, but is strongly damped. Since this mode is present only in the higher-order theories, we consider it related to gas rarefaction and speak of the rarefaction mode. In the frequency range shown, R13 and Burnett almost agree in the prediction of damping for this mode, but Burnett predicts a somewhat larger phase speed.

Interestingly, the Burnett equations predict that the damping of the rarefaction mode changes its sign at about $\omega = 5.96$ (not shown in the figure). Negative damping (or positive k_i) implies that the wave amplitude grows along the path of propagation, which is, of course, unphysical. Resonator simulations for frequencies above 5.96 show hugely overblown pressure and temperature values. This unphysicality of the Burnett equations occurs at very high frequencies, far beyond the frequency range where one would expect the Burnett equations to be valid, and we shall not show pertinent results.

4.3 Applying boundary conditions

For the application of the boundary conditions we adopt again a general notation for all four models. We note that the number of boundary conditions provided for each model equals the number ν of solutions of the dispersion relations, or wave modes. Since the various boundary conditions (5, 7, 9, 11) contain up to three space derivatives of the variables, and must be evaluated at $x = 0$ and $x = L$, we can write in compact form:

Transducer conditions, $a = 1, \ldots, \frac{\nu}{2}$:

$$\Lambda^{(0)}_{aA} u_A\,(0,t) + \Lambda^{(1)}_{aA} \frac{\partial u_A}{\partial x}\,(0,t) + \Lambda^{(2)}_{aA} \frac{\partial^2 u_A}{\partial x^2}\,(0,t) + \Lambda^{(3)}_{aA} \frac{\partial^3 u_A}{\partial x^3}\,(0,t) = F_a\,(t),$$

Receiver conditions, $a = \frac{\nu}{2} + 1, \ldots, \nu$:

$$\Lambda^{(0)}_{aA} u_A\,(L,t) + \Lambda^{(1)}_{aA} \frac{\partial u_A}{\partial x}\,(L,t) + \Lambda^{(2)}_{aA} \frac{\partial^2 u_A}{\partial x^2}\,(L,t) + \Lambda^{(3)}_{aA} \frac{\partial^3 u_A}{\partial x^3}\,(L,t) = F_a\,(t),$$

with suitable matrices $\Lambda^{(\alpha)}_{aA}$; note that the wall normal $n = \pm 1$ occurs in some elements of the $\Lambda^{(\alpha)}_{aA}$. $F_a\,(t)$ is the forcing term that contains only the wall velocities and the wall temperatures. Since the *only* forcing is the velocity of the transducer at $x = 0$, we have $F_a\,(t) = \{V_0 \cos \omega t, 0, 0, 0, \ldots\}$.

Insertion of the general solution (19) yields, after all derivatives are performed, and the time dependency is cancelled,

$$\sum_{b=1}^{\nu} \left[\Lambda^{(0)}_{aA} - i k_b \Lambda^{(1)}_{aA} - k_b^2 \Lambda^{(2)}_{aA} + i k_b^3 \Lambda^{(3)}_{aA} \right] R^b_B \alpha_b = \hat{F}_a, \tag{20}$$

$$\sum_{b=1}^{\nu}\left[\Lambda_{aA}^{(0)}-ik_b\Lambda_{aA}^{(1)}-k_b^2\Lambda_{aA}^{(2)}+ik_b^3\Lambda_{aA}^{(3)}\right]\exp\left[-ik_bL\right]R_B^b\alpha_b=\hat{F}_a, \tag{21}$$

where the first line refers to the transducer boundary ($a=1,\ldots,\frac{\nu}{2}$) and the second line refers to the receiver boundary ($a=\frac{\nu}{2}+1,\ldots,\nu$); the driving amplitude is $\hat{F}_a=\{V_0,0,0,0,\ldots\}$. This is simply an inhomogeneous linear system for the amplitude factors α_a of the form

$$\sum_{b=1}^{\nu}\mathcal{B}_{ab}\alpha_b=\hat{F}_a, \tag{22}$$

where the elements of the matrix $\mathcal{B}_{ab}$ can be read of directly from (20). Inversion of the matrix yields the amplitudes, and the solutions of all sets of equations can be written in the common compact form

$$u_A\left(x,t\right)=\sum_{a,b=1}^{\nu}R_A^a\left(\omega\right)\mathcal{B}_{ab}^{-1}\hat{F}_b\exp\left[i\left(\omega t-k_a\left(\omega\right)x\right)\right]. \tag{23}$$

The meaning of all elements in this equation is readily available from the details given in the text. We have implemented all details in a Mathematica file, which allows to plot all fields $u_A\left(x,t\right)$ for any frequency ω and any device length L.

5 Results

For all results presented, we set the Knudsen number in the equations equal to 1, so that the dimensionless frequency and the inverse dimensionless length become the relevant Knudsen numbers of the problem as discussed in Sect. 2.3. For all solutions, the velocity amplitude is set as $V_0=1$.

5.1 Receiver signal

Schotter made detailed measurements of the pressure amplitude and the phase shift at the receiver for dimensionless frequencies between 0.3 and 83.9, where he used a fixed frequency and varied pressure. Since the macroscopic models considered are only valid for sufficiently small Knudsen numbers, we consider his results only up to $\omega=1.09$ for comparison.

The receiver measures the oscillation of normal force $p+\sigma=\rho\theta+\sigma$ over the groundstate $p_0=\rho_0\theta_0$. Due to the linear regime, the oscillation is given by $P\left(t\right)=\tilde{\rho}\left(L,t\right)+\tilde{\theta}\left(L,t\right)+\tilde{\sigma}\left(L,t\right)$ and must be of the form $P\left(t\right)=P_0\cos\left(\omega t+\varphi\right)$. Schotter plotted the logarithm of the scaled amplitude $P_0$and the phase φ over scaled resonator length $\sqrt{\frac{\pi}{2}}L\omega$. Amplitude and phase can easily be extracted from our solution (23) and plotted.

In order to compare to Schotter's measurement, we copied his curves and coordinate axes into a graphics program and rescaled to the measures of the plots generated from our solutions.

In order to have a transparent presentation of all curves, curves for different ω-values were shifted vertically. The curves obtained from simulation are all shifted by the same distance, and the measurement curves were shifted to give a good fit to the simulations. Here one has some freedom, in particular the measurement curves can be shifted for good match with R13 or Burnett. In order to give a fair picture, the plots contain *two* measurement curves for the higher frequencies, one shifted to match R13 and one shifted to match Burnett.

Figure 3 shows the plots for amplitude and phase shift that were obtained in this manner. While measurements are not available for frequencies below $\omega=0.3$, we include simulations for $\omega=0.1$ and $\omega=0.2$. Again we recall that dimensionless frequency acts as Knudsen number Kn_ω and that all theories are limited to small Knudsen numbers. However, NSF is of first order in Kn, G13 and Burnett are of second order in Kn and R13 is of third order in Kn. For the smallest Knudsen number, $\omega=0.1$, all four theories yield the same results, the curves lie on top of each other. As frequency, i.e. Knudsen number, grows, the curves of the theories fan out, with R13 and Burnett giving excellent fits, NSF giving the poorest fit and G13 lying in between.

For the smallest frequencies, $\omega=0.1$ and 0.2, we recognize distinct peaks and valleys in the amplitude which are due to resonance, that is positive and negative interference with the wave reflected at the receiver. As

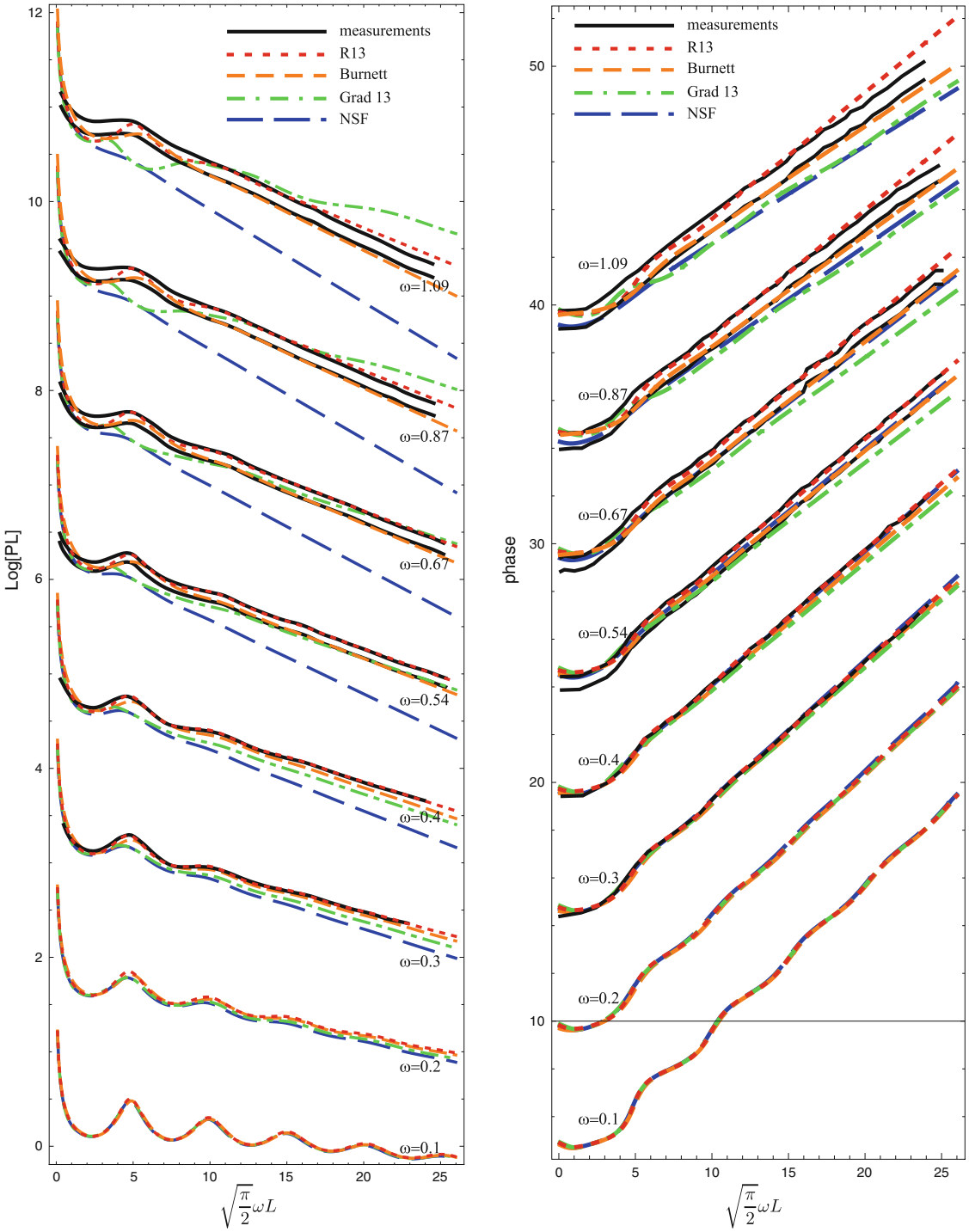

Fig. 3 Amplitude and phase shift at the receiver as function of dimensionless length $\sqrt{\frac{\pi}{2}}L\omega$. Computations for NSF (*blue, long dashes*), Burnett (*orange, dashes*), G13 (*green, dash-dots*) and R13 (*red, short dashes*) are compared to measurements (*black, continuous*) by Schotter [23] for dimensionless frequencies ω between 0.1 and 1.09. For frequencies $\omega = 0.54$ and higher two measurement curves are shown, one shifted to match Burnett, the other to match R13, see the text for details (colour figure online)

frequency grows, the peaks for larger resonator length ($L\omega$) cannot be seen anymore. Indeed, as Fig. 2 shows, damping of all modes grows considerably with frequency. Thus, there is so much damping in the rarefied gas that the amplitude of the reflected signal is too weak to play a significant role, and resonance is observed only

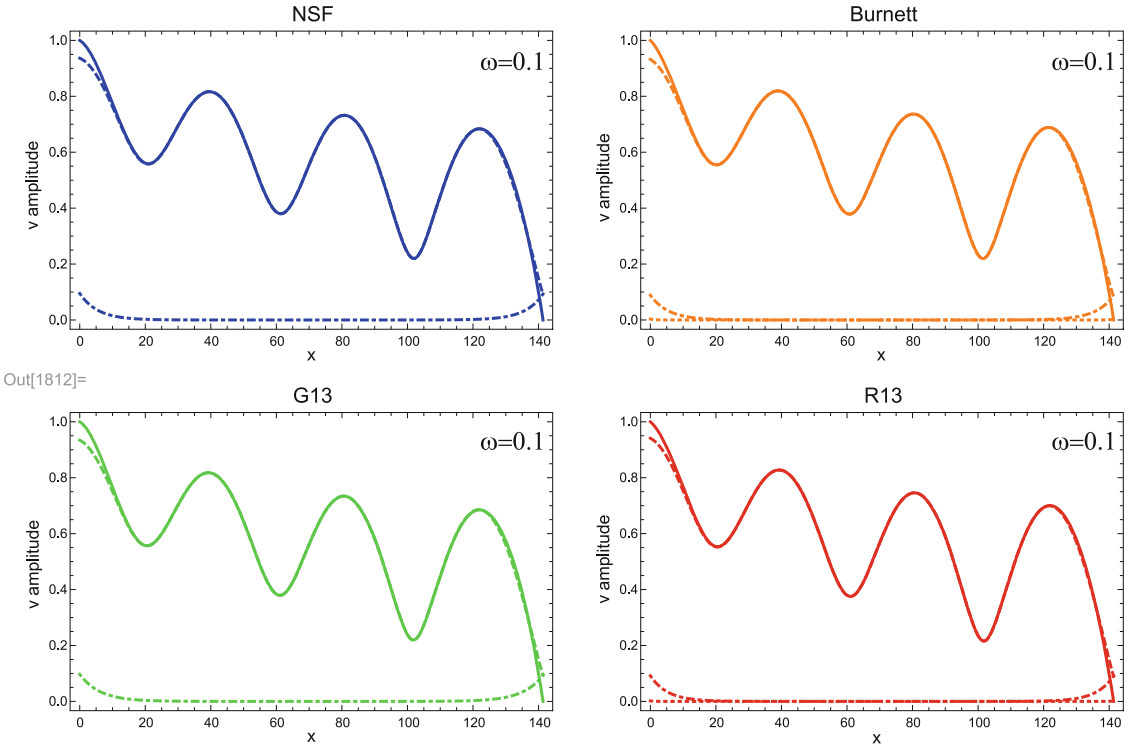

Fig. 4 $\omega = 0.1$: Velocity amplitude as function of space coordinate (*continuous curves*) together with the amplitudes for the different modes of the dispersion relation: acoustic mode (*dashed*), diffusion mode (*dash-dotted*), rarefaction mode (*dotted*)

for smaller values of $L(\sqrt{\frac{\pi}{2}}\omega L \simeq 5)$. The tail of the curves for larger L is dominated by damping which determines the slope.

For very small L, the computed pressure values lie well above those measured. As stated in Sect. 2.3, the inverse dimensionless length is another Knudsen number of the problem. Thus, small L corresponds to large Kn_L. Since all models are valid only for smaller Kn, they cannot be expected to give good results for small L. All theories considered describe the gas as a continuum, that is the collective behaviour of the gas. For these extremely small scales, however, particles are freely flying between transducer and receiver, and the macroscopic description cannot describe the individual behaviour of these particles.

In summary, we observe that the R13 and Burnett equations give excellent agreement with the measurements for frequencies up to 0.87 or even 1.09, as long as the distance L between transducer and receiver is sufficient. We emphasize that some arbitrariness is involved in shifting the experimental curves. The theoretical curves show clear differences in the actual curves between R13 and Burnett which were produced with the same boundary data. Since the measurements are given on arbitrary axes, they had to be shifted, and the actual amount of shift required cannot be reconstructed from Schotter's paper [23]. We recall that R13 is of third order in Kn and Burnett is of second order in Kn. Thus, one would expect R13 to give a better fit up to higher frequencies.

The first-order NSF equations already fail for the relatively small frequency of $\omega = 0.3$, a simple reflection of the limits of classical first-order hydrodynamics.

Considering that the Burnett equations can be derived by Chapman–Enskog expansion of the G13 equations, the latter give surprisingly low accuracy. For all frequencies from $\omega = 0.3$ onward their results have distinctively lower accuracy than Burnett.

5.2 Amplitudes and modes

The calculations also allow us to have a look at data that are not accessible to measurements. Figures 4, 5 and 6 show the local velocity amplitude over the space coordinate together with the local amplitudes for each

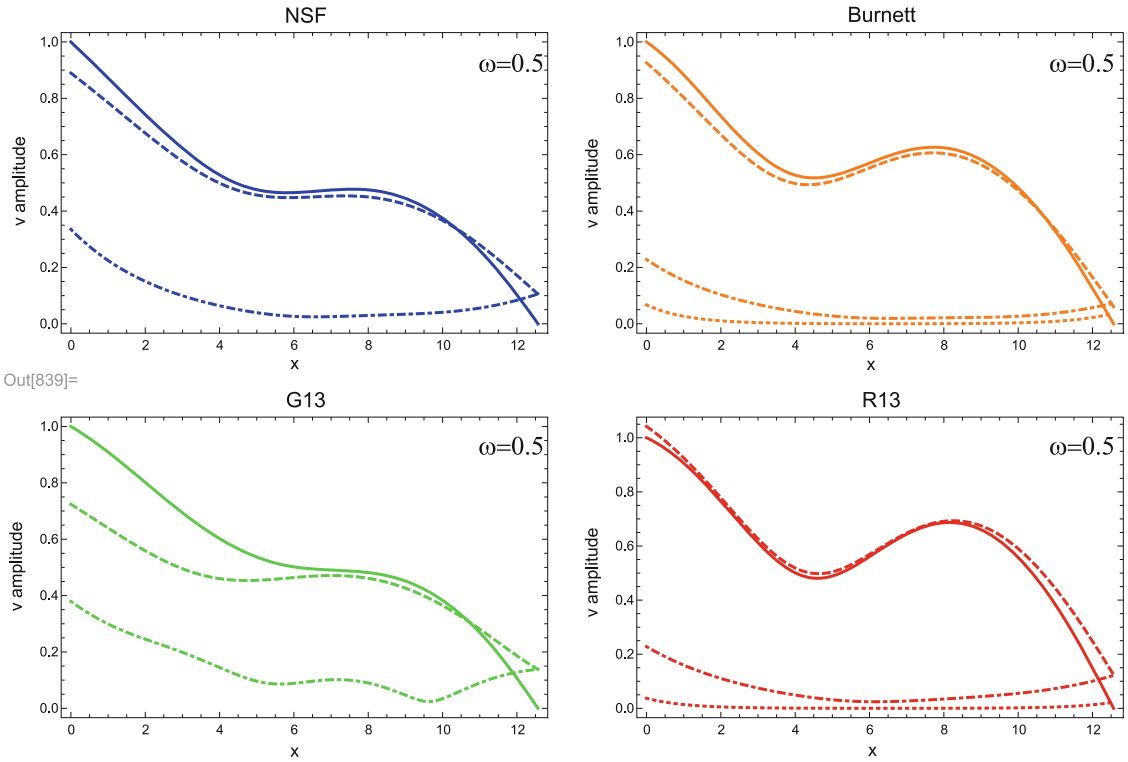

Fig. 5 $\omega = 0.5$: Velocity amplitude as function of space coordinate (*continuous curves*) together with the amplitudes for the different branches of the dispersion relation: acoustic mode (*dashed*), diffusion mode (*dash-dotted*), rarefaction mode (*dotted*)

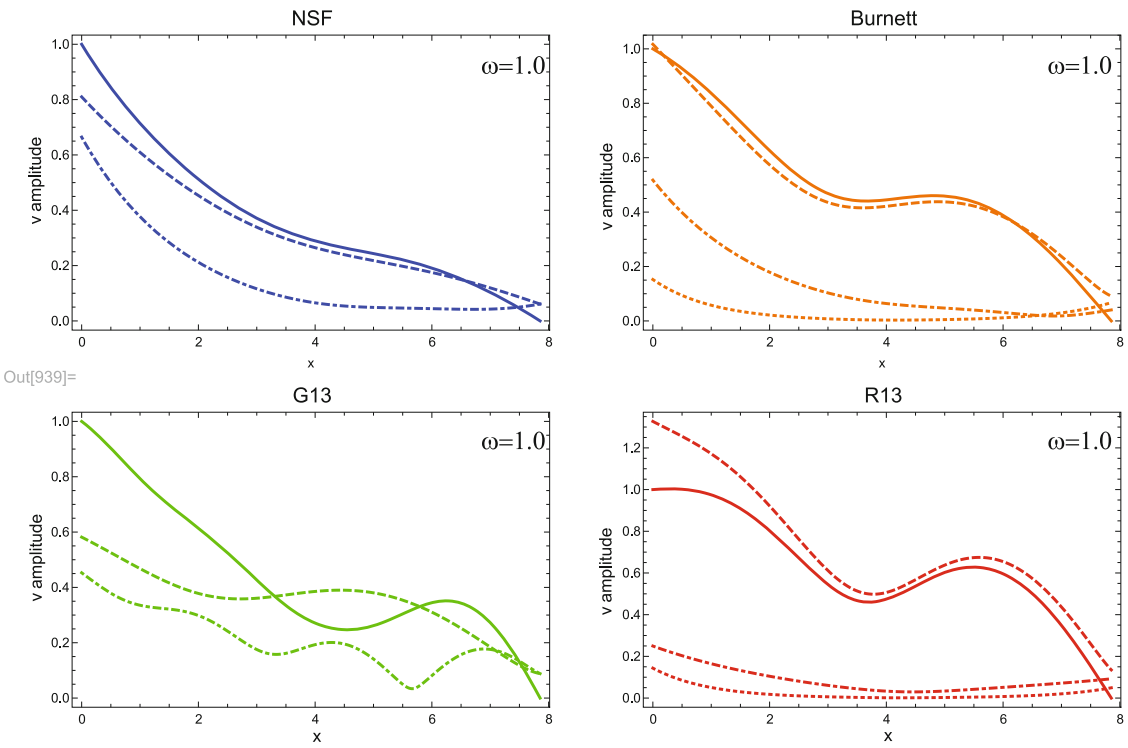

Fig. 6 $\omega = 1.0$: Velocity amplitude as function of space coordinate (*continuous curves*) together with the amplitudes for the different branches of the dispersion relation: acoustic mode (*dashed*), diffusion mode (*dash-dotted*), rarefaction mode (*dotted*)

of the modes. For better appreciation we point out that the individual modes have phase shifts against each other. Therefore, the individual modes reach their local maximum (i.e. the full amplitude) at different times. Accordingly, the amplitudes of the modes do not add up to the total amplitude, which is smaller than the sum of amplitudes.

In Fig. 4 the frequency is relatively small, at $\omega = 0.1$, and the distance is relatively large, at $L = 140$, a case where the Knudsen number is small and all theories give the same results. We see a clear wave structure, although the wave is not standing, due to damping (acoustic wave length is $\lambda = \sqrt{\frac{5}{3}}\frac{2\pi}{\omega} \simeq 81$). It can be seen that the diffusion mode (dash-dotted) contributes only very little in a small area close to the walls, due to heat transfer between the gas and the walls—there is a temperature difference between the expanding/contracting gas and the walls at θ_0. The rarefaction mode (dotted, Burnett and R13 only) has zero amplitude, which corresponds well with the low degree of rarefaction, where no rarefaction effects are expected. With these two modes essentially negligible, the acoustic mode (dashed) agrees with the total signal in the bulk, i.e. a bit away from the walls. In other words, for this case only the acoustic mode is relevant, and the other modes could be ignored.

Figure 5 shows similar curves for a case where the frequency is $\omega = 0.5$, and shorter length $L = 12.5$. Again, the total amplitude is mainly identical to the amplitude of the acoustic mode, but for all models we observe a distinct contribution of the diffusion mode. The rarefaction mode contributes almost nothing to the Burnett and R13 results. For the G13 equations, the diffusive mode shows a bit of a resonance, which is due to the sound-like character that the mode assumes for larger ω.

Finally, Fig. 6 shows the amplitudes for an even higher frequency, $\omega = 1.0$, and shorter distance, $L = 8$. Differences between the theories are quite distinct. Due to the strong damping predicted, NSF does not show a wave structure at all. G13, on the other hand, predicts a superposition of two waves with different wavelengths. R13 predicts a more pronounced wave than Burnett. In all cases, the diffusive mode is clearly excited, and the contribution of the rarefaction mode (Burnett and R13 only) cannot be ignored any more. Due to lack of data for comparison, we cannot judge whether the R13 or Burnett prediction is more reliable.

5.3 Overall damping and velocity

Experimentally, one determines phase speed and damping by assuming that the pressure signal in the resonator is a single damped wave of the form (13),

$$P\,(x,t) = A\exp\left[k_i x\right]\cos\left[\omega t - k_r x + \varphi\right]. \tag{24}$$

Considering this equation for two locations X_1 and X_2, one finds

$$k_r = \frac{\arccos\frac{P(X_1,0)}{P(X_1,t_1)} - \arccos\frac{P(X_2,0)}{P(X_2,t_1)}}{X_2 - X_1}, \quad k_i = \frac{\ln\frac{P(X_2,t_2)}{P(X_1,t_1)}}{X_2 - X_1} \tag{25}$$

where $t_{1,2}$ are the times where $\cos[\omega t - k_r X_{1,2} + \varphi] = 0$. Thus, the elements of the complex wave vector can be determined from the slopes (properly rescaled) of the curves shown in Fig. 3. In the measurement, X_1 and X_2 are, in fact, different resonator lengths.

While our analytical result is a superposition of damped waves, we can use the above method to determine overall values for k_r and k_i from the solution. In other words, we consider the computed curves in Fig. 3 and determine the overall wave vector from the slopes of the curves. Clearly, one has to use the right end of the curves (i.e. longer resonators), so that resonance does not affect the outcome. Results of this procedure for phase velocity $v_{ph} = \frac{\omega}{k_r}$ and k_i are shown in Figs. 7 and 8 for the four theories under consideration (dots), together with experimental data (diamonds, [25]) and the curves for the different branches of the dispersion relation. The latter are the same as in Fig. 2, only that the frequency range is extended, and the frequency axis is logarithmic.

The dots in Fig. 7 were determined for very long resonators ($\sqrt{\frac{\pi}{2}}L\omega \simeq 275$). One sees nicely that the overall results (dots) agree perfectly with that mode of the dispersion relation that has the lowest damping. For NSF, Grad13 and R13, this is always the sound mode, but for Burnett, there is a switch between sound mode and diffusion mode at about $\omega \simeq 2$.

Somewhat surprisingly, the Burnett sound mode gives the damping k_i in good agreement with experimental data for the whole frequency range shown. However, the result shows that above $\omega \simeq 2$ the sound mode is not relevant for the prediction.

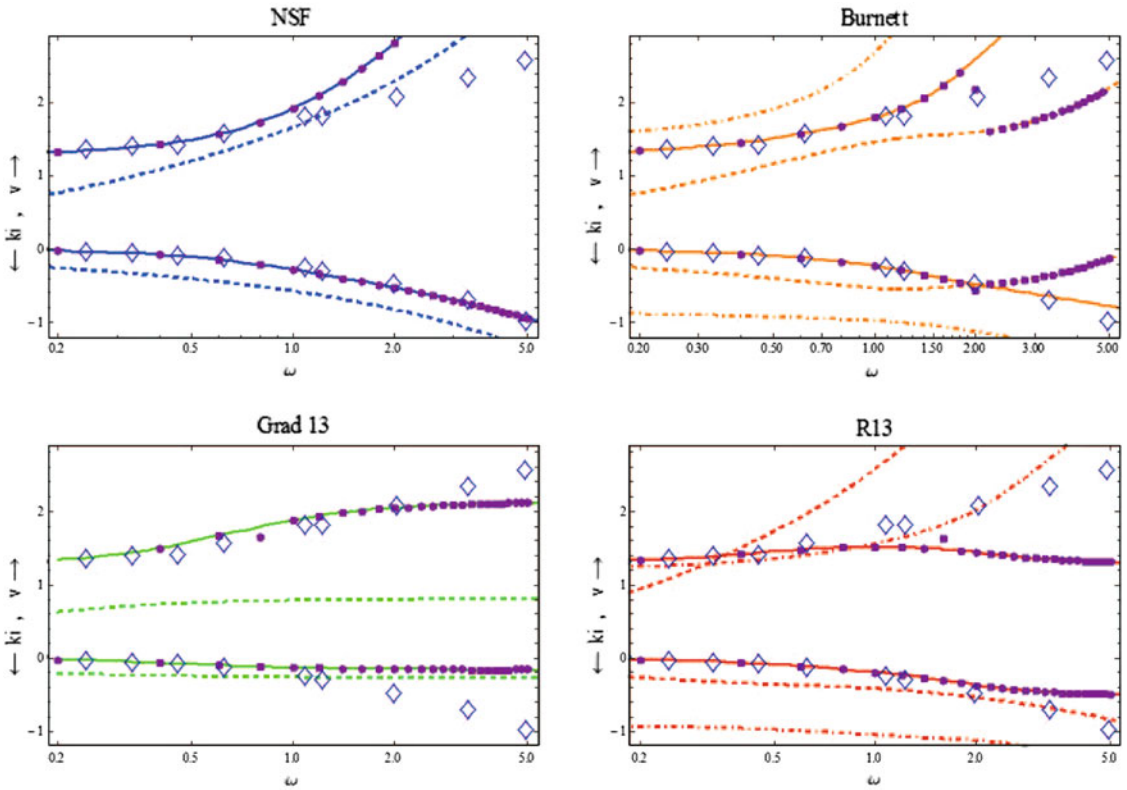

Fig. 7 Phase velocity and damping for the various theories plotted together with experimental data (*diamonds*, [25]) and average values determined from the slopes of damping and phase (*dots*). The branches of the dispersion relation are shown as lines, as in Fig. 2. These curves are for very long resonator

Figure 8 shows data for shorter resonators ($\sqrt{\frac{\pi}{2}}L\omega \simeq 27.5$). For NSF and R13 the overall wave vector follows essentially the sound mode, but for Burnett and G13 we observe more marked deviations which are due to the superpositions of several important branches of the dispersion relation. Due to the scale, it is somewhat difficult to compare the predictions of the various theories for wave speed and damping with the experimental data. Better comparison is possible when one considers the inverse dimensionless wave speed $\sqrt{\frac{5}{3}}\frac{1}{v_{ph}} = \frac{k_r}{\omega}$ and the reduced damping $\frac{k}{\omega}$ as functions of the inverse frequency $\frac{1}{\omega}$, as shown in Fig. 9 for the sound modes of all four models. One can see nicely that NSF and G13 give agreement only for smaller frequencies while Burnett and R13 give a good description for frequencies up to $\omega = 1$ or even higher.

As stated above already, it is quite surprising that Burnett gives a much better description than G13, since, indeed, Burnett can be derived from G13 through the Chapman–Enskog method.

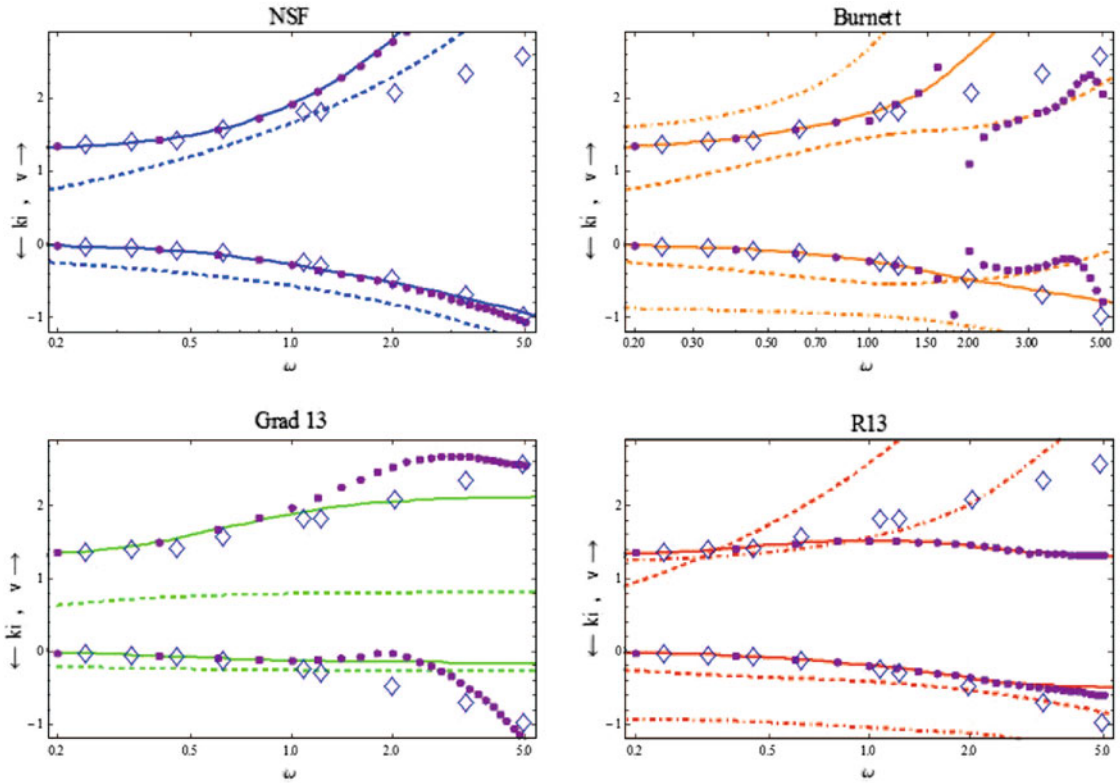

Fig. 8 Phase velocity and damping for the various theories plotted together with experimental data (*diamonds*, [25]) and average values determined from the slopes of damping and phase (*dots*). The branches of the dispersion relation are shown as lines, as in Fig. 2. These curves are for short resonator

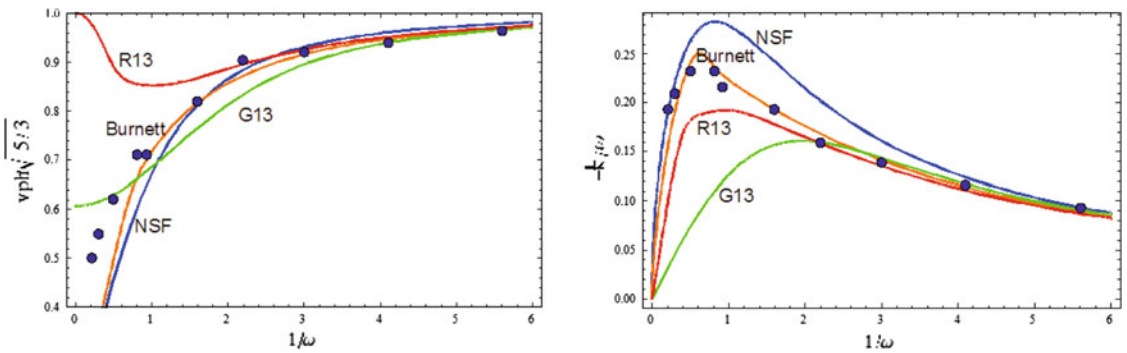

Fig. 9 Sound mode: Inverse dimensionless phase speed $\sqrt{\frac{5}{3}}\frac{1}{v_{ph}} = \frac{k_r}{\omega}$ and reduced damping $\frac{k}{\omega}$ as functions of the inverse frequency $\frac{1}{\omega}$. The points are experimental data [25]

6 Conclusion

We have considered mildly rarefied gases in resonators with the Navier-Stokes-Fourier, Burnett, G13 and R13 equations. Full solution of the resonator boundary value problem shows that all transport modes contribute to the sound propagation, but one mode, the sound mode, dominates transport, since this is the mode with lowest damping. Only shorter resonators are influenced by the other modes.

Acknowledgments This research was supported by the Natural Sciences and Engineering Research Council (NSERC).

References

1. Chapman, S., Cowling, T.G.: The Mathematical Theory of Non-Uniform Gases. Cambridge University Press, Cambridge (1970)
2. Cercignani, C.: Theory and Application of the Boltzmann Equation. Scottish Academic Press, Edinburgh (1975)
3. Sone, Y.: Kinetic Theory and Fluid dynamics. Birkhäuser, Boston (2002)
4. Struchtrup, H.: Macroscopic Transport Equations for Rarefied Gas Flows—Approximation Methods in Kinetic Theory. Interaction of Mechanics and Mathematics Series, Springer, Heidelberg (2005)
5. Struchtrup, H., Taheri, P.: Macroscopic transport models for rarefied gas flows: a brief review. IMA J. Appl. Math. (2011). doi:10.1093/imamat/hxr004
6. Burnett, D.: The distribution of molecular velocities and the mean motion in a non-uniform gas. Proc. Lond. Math. Soc. **40**, 382–435 (1936)
7. Shavaliyev, M.S.: Super-Burnett corrections to the stress tensor and the heat flux in a gas of Maxwellian molecules. J. Appl. Math. Mech. **57**(3), 573–576 (1993)
8. Bobylev, A.V.: The Chapman-Enskog and grad methods for solving the Boltzmann equation. Sov. Phys. Dokl. **27**, 29–31 (1982)
9. Müller, I., Ruggeri, T.: Rational Extended Thermodynamics. Springer, New York (Springer Tracts in Natural Philosophy vol. 37) (1998)
10. Myong, R.-S.: A computational method for Eu's generalized hydrodynamic equations of rarefied and microscale gas dynamics. J. Comput. Phys. **168**(1), 47–72 (2001)
11. Grad, H.: On the kinetic theory of rarefied gases. Commun. Pure Appl. Math. **2**, 331–407 (1949)
12. Grad, H.: Principles of the kinetic theory of gases. In: Flügge, S. (ed.) Handbuch der Physik XII: Thermodynamik der Gase, Springer, Berlin (1958)
13. Struchtrup, H., Torrilhon, M.: Regularization of grad's 13 moment equations: derivation and linear analysis. Phys. Fluids **15**(9), 2668–2680 (2003)
14. Struchtrup, H.: Stable transport equations for rarefied gases at high orders in the Knudsen number. Phys. Fluids **16**(11), 3921–3934 (2004)
15. Torrilhon, M., Struchtrup, H.: Boundary conditions for regularized 13-moment-equations for micro-channel-flows. J. Comp. Phys. **227**, 1982–2011 (2008)
16. Struchtrup, H., Torrilhon, M.: Higher-order effects in rarefied channel flows. Phys. Rev. E **78**, 046301 (2008)
17. Struchtrup, H., Torrilhon, M.: Higher-order effects in rarefied channel flows. Phys. Rev. E **78**, 069903 (2008)
18. Torrilhon, M., Struchtrup, H.: Regularized 13-moment-equations: shock structure calculations and comparison to Burnett models. J. Fluid Mech. **513**, 171–198 (2004)
19. Taheri, P., Torrilhon, M., Struchtrup, H.: Couette and Poiseuille flows in microchannels: analytical solutions for regularized 13-moment equations. Phys. Fluids **21**, 017102 (2009)
20. Taheri, P., Struchtrup, H.: Effects of rarefaction in microflows between coaxial cylinders. Phys. Rev. E **80**, 066317 (2009)
21. Taheri, P., Struchtrup, H.: An extended macroscopic transport model for rarefied gas flows in long capillaries with circular cross section. Phys. Fluids **22**, 112004 (2010)
22. Weiss, W.: Zur Hierarchie der Erweiterten Thermodynamik. Ph.D. Thesis, Technical University, Berlin (1990)
23. Schotter, R.: Rarefied acoustics in the noble gases. Phys. Fluids **17**, 1163–1168 (1974)
24. Maxwell, J.C.: On stresses in rarefied gases arising from inequalities of temperature. Phil. Trans. Roy. Soc. (London) **170**, 231–256 (1879)
25. Meyer, E., Sessler, G.: Schallausbreitung in Gasen bei hohen Frequenzen und sehr niedrigen Druecken. Zeitschr. Physik. **149**, 15–39 (1957)